Applied Physics Letters

Local anisotropy control of Pt/Co/Ir thin film with perpendicular magnetic anisotropy by surface acoustic waves

Cite as: Appl. Phys. Lett. **120**, 252402 (2022); https://doi.org/10.1063/5.0097172
Submitted: 26 April 2022 • Accepted: 09 June 2022 • Published Online: 21 June 2022

Jintao Shuai, Mannan Ali, Luis Lopez-Diaz, et al.

Applied Physics Letters ARTICLE scitation.org/journal/apl

Local anisotropy control of Pt/Co/Ir thin film with perpendicular magnetic anisotropy by surface acoustic waves

Cite as: Appl. Phys. Lett. **120**, 252402 (2022); doi: 10.1063/5.0097172
Submitted: 26 April 2022 · Accepted: 9 June 2022 ·
Published Online: 21 June 2022

View Online Export Citation CrossMark

Jintao Shuai,[1] Mannan Ali,[1] Luis Lopez-Diaz,[2] John E. Cunningham,[3,a)] and Thomas A. Moore[1,a)]

AFFILIATIONS

[1]School of Physics and Astronomy, University of Leeds, Woodhouse Lane, Leeds LS2 9JT, United Kingdom
[2]Department of Applied Physics, Universidad de Salamanca, Salamanca, Spain
[3]School of Electronic and Electrical Engineering, University of Leeds, Woodhouse Lane, Leeds LS2 9JT, United Kingdom

[a)]Authors to whom correspondence should be addressed: J.E.Cunningham@leeds.ac.uk and T.A.Moore@leeds.ac.uk

ABSTRACT

The control of perpendicular magnetic anisotropy (PMA) in thin films by strain has considerable potential for energy-efficient information storage and data processing. Here, we report on the control of PMA in Pt/Co/Ir thin films by the strain produced by standing surface acoustic waves (SAWs). A significant (~21%) coercivity reduction (from 4.80 ± 0.03 to 3.80 ± 0.02 mT) can be obtained by applying a standing SAW with a center frequency of 93.35 MHz. Furthermore, the standing SAWs induce a greater-than 11-fold increase in magnetization reversal speed (from 168 ± 3 to up to 2100 ± 80 $\mu m^2/s$) at 3.2 mT for a total applied RF power of 22.5 dBm. During application of SAWs, wide-field Kerr microscopy reveals the formation of domains in stripes with a periodicity of half of the SAW wavelength. Micromagnetic simulations indicate that the anti-nodes of the standing SAW locally lower the anisotropy due to the magneto-elastic coupling effect, decreasing domain nucleation field while promoting magnetization reversal. Our study suggests the possibility of remote and energy-efficient control of magnetization switching using SAWs.

Materials with strong perpendicular magnetic anisotropy (PMA) are promising candidates for future generations of data storage and processing devices owing to their stable magnetization states and narrow domain walls.[1–4] These features confer stability of the stored information while providing a high storage density.[5] However, unfortunately, materials with strong PMA typically also require a large current to reverse the magnetization or to move domain walls in order to write or transfer data, which can itself cause energy wastage and Joule heating, so limiting the packing density of useful devices.[6,7] There is much interest in reducing the energy required to manipulate domain walls, for instance, by electric field or by strain.[8–13]

Owing to the magneto-elastic coupling effect, one can introduce strain to modify the PMA in a magnetic thin film by applying voltage to an adjacent piezoelectric material. For example, Shepley *et al.* modified Pt/Co/Pt thin films with PMA by applying static strain using dc voltage applied to a piezoelectric transducer. The static strain reduced the coercivity and increased the domain wall creep velocity by up to 100%.[14] Ranieri *et al.* demonstrated a 5% anisotropy reduction in out-of-plane anisotropy resulting in a 500% domain wall mobility variation in a perpendicularly magnetized GaMnAsP/GaAs ferromagnetic semiconductor by using a piezoelectric stressor.[15] Gopman *et al.* reduced the coercivity of Co/Ni multilayers more than 30% by expanding the $Pb(Zr_{0.52}Ti_{0.48})O_3$ by 0.1%.[11]

Surface acoustic waves (SAWs) are acoustic waves traveling along the surface of a material exhibiting elasticity, which can introduce time-varying (dynamic) strain waves in the magnetic thin films.[16–21] Dean *et al.* simulated the remote introduction of an array of attractive domain wall pinning sites by forming a standing strain wave showing theoretically that multiple domain walls could be synchronously moved by shifting the frequency of the SAW.[22] Adhikari *et al.* reported that a SAW can depin magnetic domain walls, increasing the probability of depinning between 4 and 9 times and increasing the domain wall velocity in Co/Pt multilayers up to eight times.[19,20] Thevenard *et al.* experimentally demonstrated up to 60% coercivity reduction in an out-of-plane magnetized (Ga,Mn)(As,P) films at ~40 K, showing the potential of SAW-assisted magnetization switching.[17] SAW-induced coercivity reduction and domain wall motion show significant potential for energy-efficient information storage and data processing devices, since the magnetization switching is driven by voltage instead of current. However, the SAW-induced (dynamic strain) magnetization switching mechanism of thin films with PMA remains unclear, especially the role of the nodes and anti-nodes of the standing SAW in the magnetization reversal process. Moreover, the correlation between the properties of SAWs and magnetization changes also is uncertain.

In the current study, we demonstrate local anisotropy control of a Ta/Pt/Co/Ir/Ta thin film with PMA by standing SAWs at a center frequency of 93.35 MHz. In the presence of a SAW, the coercivity of the thin films significantly decreases, while the magnetization reversal speed increases. These experimental results, along with micromagnetic simulations, reveal that the anti-nodes of the standing SAWs locally reduce the anisotropy of the Pt/Co/Ir thin film, which lowers the coercivity and favors magnetization reversal.

Figures 1(a) and 1(b) show a schematic of the experimental arrangement comprising a 2-mm-wide stripe of Ta(5.0)/Pt(2.5)/Co(1.1)/Ir(1.5)/Ta(5.0) [for nominal thicknesses in nm, see Fig. 1(a)] thin film with PMA prepared by dc magnetron sputtering onto an 128° Y-cut lithium niobate ($LiNbO_3$) substrate. The base pressure during the thin film preparation was below 3.0×10^{-6} Pa. As shown in Fig. 1(b), one pair of Ti(10 nm)/Au(90 nm) interdigitated transducers (IDTs), each consisting of 20 pairs of electrodes, was patterned using optical lithography (exposure of the resist was achieved using a maskless laser aligner, with subsequent metal evaporation and liftoff forming the IDTs). The aperture of the IDTs and the SAW propagation distance were 450 and 3 mm, respectively. The finger width and spacing were both designed to be 10 μm. A vector network analyzer (Agilent E5062A) was first used to obtain the S-parameters. Figure 1(c) shows the reflection (S11 and S22) and transmission (S21 and S12) characteristics of the SAW transducers and substrate showing a center frequency of 93.35 MHz, yielding a wavelength of 42.667 $\pm$ 0.004 μm [the accuracy of the frequency from VNA is 5 ppm, and the propagating velocity of SAW on $LiNbO_3$ is 3982 m/s (Ref. 23)]. A description of the RF circuit used to apply signals to generate the SAWs is given in the supplementary material. A wide-field Kerr microscope with a 50$\times$ objective lens and field applied out of the film plane was used to measure the hysteresis loops, image the domain patterns, and determine the magnetization reversal speed of the thin films. To determine the magnetization reversal speed, a pulsed field was applied to the thin film to switch the magnetization, while the magnetization reversal speed was determined by the area of the reversed magnetization divided by the pulse width. Details about the determination of magnetization reversal speed can be found in the supplementary material. Five individual tests for all experiments were conducted and averaged.

Figure 2(a) shows the hysteresis loops of the thin films for different applied SAW power from 17.5 to 22.5 dBm (at 93.35 MHz) and also without SAW. The sharp switching of the magnetization indicates a strong perpendicular magnetic anisotropy of the Co layer. The presence of the curved corners is because a higher (than coercivity) field is required to squeeze out the homochiral domain walls to saturate the thin film.[24] Significant coercivity reduction was observed in the presence of the standing SAW: the coercivity decreases with increasing applied power from 4.46 $\pm$ 0.04 mT at 17.5 dBm to 3.80 $\pm$ 0.02 mT at 22.5 dBm [Figs. 2(b) and 2(c)]. The coercivity is, thus, up to $\sim$21% reduced compared to that measured without SAW (4.80 $\pm$ 0.03 mT). The coercivity reduction can be explained by the strain-induced changes of the PMA.[14] SAWs act as time-varying strain waves, which can locally change the energy landscape of the thin films, periodically raising and lowering the anisotropy of the thin film. The magnetization reverses when the anisotropy is at low values. Due to the nature of the magnetization reversal process, the magnetization is not irreversible even when the anisotropy is at the highest value. The anisotropy changes increase with the increasing applied powers. It is worth noting that the introduction of the RF power used to generate the SAW could potentially increase the temperature, which could also lower the coercivity. We, therefore, investigated the effect of changing the frequency used to generate the SAWs for the same applied power level [Figs. 2(d)–2(f)]. The coercivity reduction gradually increases when the frequency approaches the center frequency and reaches a minimum coercivity at the center frequency following the same trend as the S21 curves [overlaid on the coercivity in Fig. 2(f)], thus indicating that the coercivity reduction is caused directly by the standing SAW instead of RF power induced heating. SAW-induced temperature changes are negligible, which has been reported in Refs. 17, 25, and 26 using a similar setup and power level.

Figures 3(a)–3(c) show the influence of the external field, applied SAW power, and the frequency of the SAW on the magnetization

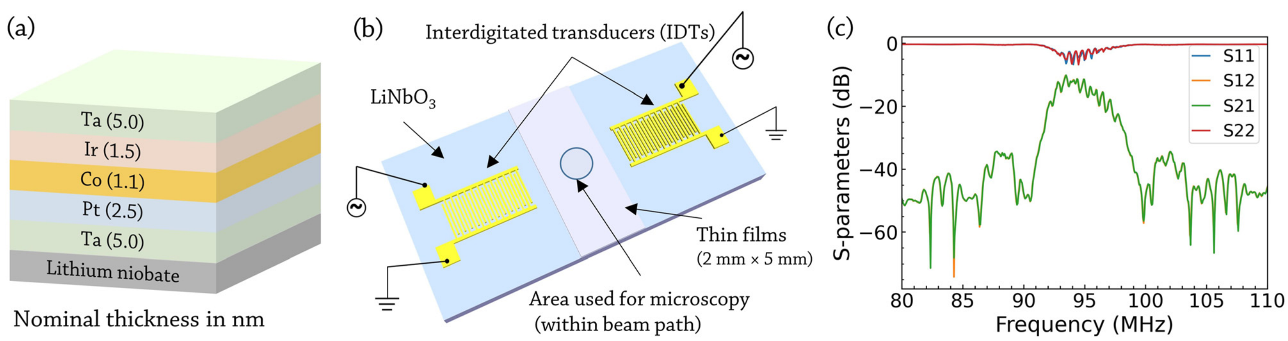

FIG. 1. (a) Thin film structure: Ta(5.0)/Pt(2.5)/Co(1.1)/Ir(1.5)/Ta(5.0) (nominal thickness in nm). (b) Schematic of the experimental arrangement (not to scale). The 2-mm-wide thin film was dc sputtered onto the lithium niobate substrate. An interdigitated transducer (IDT) was patterned each side of the thin film to launch the SAWs. (c) Scattering parameters (S-parameters) of the interdigitated transducers. The delay line comprising both IDTs and the substrate shows a center frequency of 93.35 MHz, and 3 dB bandwidth of 9.34 MHz.

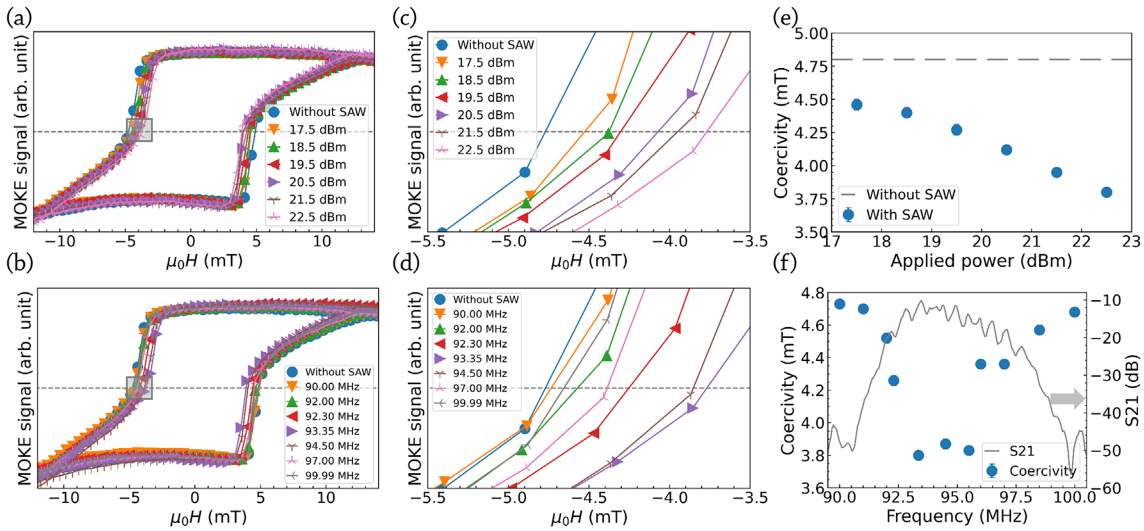

FIG. 2. Hysteresis loops of the thin films measured by Kerr microscopy across applied SAW power from 17.5 to 22.5 dBm (a) and SAW frequency from 90.00 to 99.99 MHz (b). (c) and (d) are the enlarged views of the framed areas in (a) and (b), respectively. Coercivity against applied power (e) and frequency (f). S21 is also displayed in (f). The frequency of SAW in (a), (c), and (e) is 93.35 MHz. The applied SAW power in (b), (d), and (f) is 22.5 dBm. Error bars in (e) and (f) are smaller than the data points. Lines in (a)–(d) are guides to the eye.

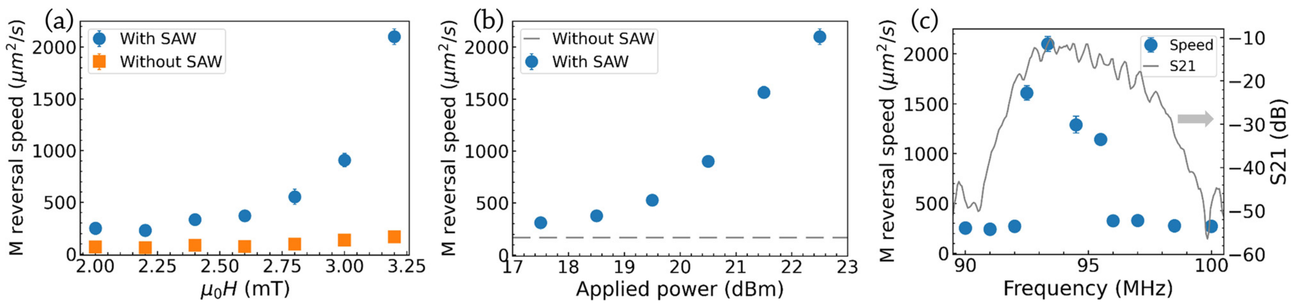

FIG. 3. Magnetization reversal speed against external magnetic field (a), applied power (b), and frequency (c) of the standing SAW. The applied power and frequency of SAW in (a) are 22.5 dBm and 93.35 MHz, respectively. The external field and frequency of SAW in (b) are 3.2 mT and 93.35 MHz, respectively. The external field and applied power of SAW in (c) are 3.2 mT and 22.5 dBm, respectively.

reversal speed, respectively. As shown in Fig. 3(a), with the external magnetic field increasing from 2.0 to 3.2 mT, the changes of the magnetization reversal speed without SAW are very limited (from 71 ± 5 to 168 ± 3 $\mu m^2/s$), whereas in the presence of the standing SAW, the magnetization reversal speed increases from 249 ± 20 $\mu m^2/s$ at 2.0 mT to 2100 ± 80 $\mu m^2/s$ at 3.2 mT, which is a ∼740% increase. The magnetization reversal speed is increased eleven-fold at 3.2 mT in the SAW's presence compared to that with magnetic field only. The implication is that the standing SAW can significantly lower the required switching field and accelerate the magnetization reversal. At 93.35 MHz, the magnetization reversal speed gradually increases with the increasing applied SAW power from 310 ± 30 $\mu m^2/s$ at 17.5 dBm to 2100 ± 80 $\mu m^2/s$ at 22.5 dBm with a 3.2 mT field [see Fig. 3(b)]. Similar to the effect of frequency on the coercivity reduction, the magnetization reversal speed increases when the frequency approaches the center frequency, achieving its maximum value near the center frequency [as shown in Fig. 3(c)]. We note that the S21 response is asymmetric and biased toward better transduction at lower frequencies, resulting in the biased magnetization reversal speed. The change of the magnetization reversal speed is caused by two main factors. First, the presence of the standing SAW significantly reduces the domain nucleation field owing to the magneto-elastic coupling effect [see Fig. 2(a)]. Meanwhile, the SAW induced anisotropy changes accelerate the domain wall velocity. The domain wall energy can be expressed as $\gamma = \sqrt{AK_{eff}}$, where A is the exchange stiffness and K_{eff} is the effective anisotropy. SAW locally and periodically lower the anisotropy of the thin film, which benefits the domain wall motion.[14]

Figures 4(a) and 4(b) show domain patterns with both SAW on and off obtained using Kerr microscopy. A 50 mT out-of-plane magnetic field was first applied to the sample to saturate the magnetization in the "up" direction. A 4.6 mT field was then applied in the opposite direction. A large number of small branch domains nucleated and propagated randomly in the thin film without the SAW [see Fig. 4(a)]. With the application of a standing SAW, the required domain nucleation field was much lower (around 3.6 mT for an applied power of 22.5 dBm at the center frequency of 93.35 MHz). The domains tended

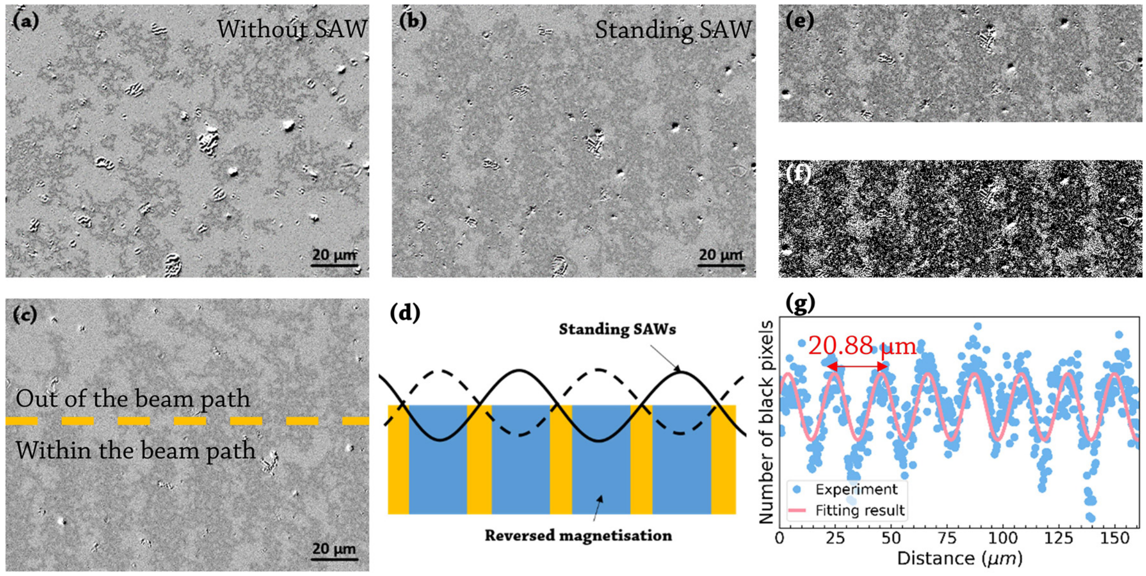

FIG. 4. (a) Domain patterns with only magnetic field (4.6 mT), (b) domain patterns with both magnetic field (3.6 mT) and 93.35 MHz standing SAW at 22.5 dBm, (c) domain patterns at the boundary of the beam path, (d) schematic of the standing SAW-assisted magnetization reversal, (e) cropped image from (b), (f), and (e) in binary value, and (g) the number of black pixels in (f) and its sinusoidal fitting. The fitting results show a wavelength of ∼20.88 μm, which is very close to the half-wavelength of the standing SAW (∼21 μm).

to nucleate in certain parts of the thin film and line up forming a clear stripe pattern [as shown in Fig. 4(b)]. The alignment of the domain patterns only occurs within the SAW beam path, with a random distribution of domains observed outside of the beam path [Fig. 4(c)]. This result itself indicates very strongly that the standing SAWs are responsible for the domain patterns. Figure 4(e) is cropped from Fig. 4(b). By converting Fig. 4(e) into binary value [Fig. 4(f)] and counting the number of the black pixels, we plotted the distribution of the domains [see Fig. 4(c)]. The experimental data were fitted by a sinusoidal function. The fit shows that the spacing between the lines is $20.88 \pm 0.06\,\mu$m, corresponding well to the nominal half-wavelength (∼21.33 μm) spacing expected of the standing SAW. This is because the magneto-elastic coupling effect will be the strongest at anti-nodes of the standing SAW, where the surface deflection is largest and where the local lowering the anisotropy is expected to be the greatest. The effect is expected to be the weakest at the nodes of the standing SAW [as depicted in Fig. 4(d)].

To further understand the effect of the nodes and anti-nodes of the standing SAW on the magnetization reversal process, we performed micromagnetic simulations using Mumax3 with a built-in strain tensor.[27] The configuration of the micromagnetic simulations can be found in the supplementary material. As shown in Fig. 5(a), the red, white, and blue indicate strains with maximum, zero, and minimum values, respectively. The system was first relaxed with magnetization pointing "down" [see Fig. 5(b)]. Standing SAWs ($\varepsilon_{max} = 0.06$) together with the external magnetic field (300 mT) pointing up were then applied. As shown in Fig. 5(c), at 1.5 ns, domains begin nucleating at the anti-nodes of the standing SAW. Then, the domains continue nucleating and propagating from anti-nodes to nodes until the domains merge with each other [Figs. 5(d) and 5(e)], followed by domain propagation out of the beam path [Fig. 5(f)]. The simulation results agree qualitatively with our experiments and in particular, our

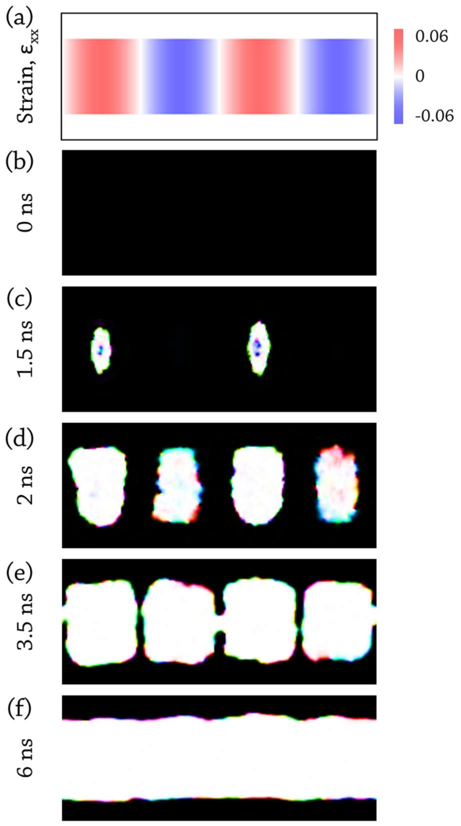

FIG. 5. (a) Spatial strain profile and (b)–(f) magnetization at 0, 1.5, 2, 3.5, and 6 ns after applying field (300 mT) and standing SAW, respectively. The black and white colors in (b)–(f) represent magnetization pointing "down" and "up," respectively.

assumption that the anti-nodes of the standing SAW favor the nucleation of the domains and the propagation of the domain walls. The simulation and magnetization reversal speed results also reveal that standing SAWs lower the coercivity of the thin films by lowering the local domain nucleation field and accelerating domain wall propagation.

In conclusion, a strong coercivity reduction (up to ~21%) was observed for the Ta/Pt/Co/Ir/Ta thin films with perpendicular magnetic anisotropy upon application of 93.35 MHz standing SAWs. Due to the SAW-induced magneto-elastic coupling effect, the magnetization reversal speed was significantly enhanced (by a factor of 11). The experiments and Mumax simulations together indicate that owing to the strain distribution difference, standing SAWs are able to lower the domain nucleation field locally at the anti-nodes of the standing SAW. Domains tended to nucleate and propagate from anti-nodes to nodes of the standing SAW, forming striped domain patterns with spacing the same as the half-wavelength of the standing SAW.

See the supplementary material for the RF circuit used to generate SAWs, the determination of the magnetization reversal speed, and the configuration of the micromagnetic simulations. Data associated with this paper are available from the Research Data Leeds repository at https://doi.org/10.5518/1169.

The authors gratefully acknowledge funding from the European Union's Horizon 2020 research and innovation program under the Marie Sklodowska-Curie Grant Agreement No. 860060 "Magnetism and the effect of Electric Field" (MagnEFi). The authors gratefully acknowledge Dr. Li Chen for the interdigitated transducer fabrication.

AUTHOR DECLARATIONS

Conflict of Interest

The authors have no conflicts to disclose.

Author Contributions

Jintao Shuai: Data curation (equal); Formal analysis (equal); Investigation (equal); Methodology (equal); Writing – original draft (equal). **Mannan Ali:** Methodology (equal). **Luis Lopez-Diaz:** Conceptualization (equal); Resources (equal); Software (equal); Writing – review and editing (equal). **John E. Cunningham:** Conceptualization (equal); Investigation (equal); Resources (equal); Supervision (equal); Validation (equal); Writing – review and editing (equal). **Thomas A. Moore:** Conceptualization (equal); Funding acquisition (equal); Investigation (equal); Methodology (equal); Project administration (equal); Resources (equal); Supervision (equal); Writing – review and editing (equal).

DATA AVAILABILITY

The data that support the findings of this study are available from the corresponding authors upon reasonable request.

REFERENCES

[1]S.-W. Jung, W. Kim, T.-D. Lee, K.-J. Lee, and H.-W. Lee, "Current-induced domain wall motion in a nanowire with perpendicular magnetic anisotropy," Appl. Phys. Lett. **92**, 202508 (2008).
[2]S. S. Parkin, M. Hayashi, and L. Thomas, "Magnetic domain-wall racetrack memory," Science **320**, 190–194 (2008).
[3]S. Emori, U. Bauer, S.-M. Ahn, E. Martinez, and G. S. Beach, "Current-driven dynamics of chiral ferromagnetic domain walls," Nat. Mater. **12**, 611–616 (2013).
[4]K.-S. Ryu, L. Thomas, S.-H. Yang, and S. Parkin, "Chiral spin torque at magnetic domain walls," Nat. Nanotechnol. **8**, 527–533 (2013).
[5]B. Dieny and M. Chshiev, "Perpendicular magnetic anisotropy at transition metal/oxide interfaces and applications," Rev. Mod. Phys. **89**, 025008 (2017).
[6]I. M. Miron, T. Moore, H. Szambolics, L. D. Buda-Prejbeanu, S. Auffret, B. Rodmacq, S. Pizzini, J. Vogel, M. Bonfim, A. Schuhl *et al.*, "Fast current-induced domain-wall motion controlled by the Rashba effect," Nat. Mater. **10**, 419–423 (2011).
[7]A. Yamaguchi, S. Nasu, H. Tanigawa, T. Ono, K. Miyake, K. Mibu, and T. Shinjo, "Effect of Joule heating in current-driven domain wall motion," Appl. Phys. Lett. **86**, 012511 (2005).
[8]F. Matsukura, Y. Tokura, and H. Ohno, "Control of magnetism by electric fields," Nat. Nanotechnol. **10**, 209–220 (2015).
[9]G. Radaelli, D. Petti, E. Plekhanov, I. Fina, P. Torelli, B. Salles, M. Cantoni, C. Rinaldi, D. Gutiérrez, G. Panaccione *et al.*, "Electric control of magnetism at the Fe/$BaTiO_3$ interface," Nat. Commun. **5**, 3404 (2014).
[10]C. Song, B. Cui, F. Li, X. Zhou, and F. Pan, "Recent progress in voltage control of magnetism: Materials, mechanisms, and performance," Prog. Mater. Sci. **87**, 33–82 (2017).
[11]D. B. Gopman, C. L. Dennis, P. Chen, Y. L. Iunin, P. Finkel, M. Staruch, and R. D. Shull, "Strain-assisted magnetization reversal in Co/Ni multilayers with perpendicular magnetic anisotropy," Sci. Rep. **6**, 27774 (2016).
[12]Y. Shirahata, R. Shiina, D. L. González, K. J. Franke, E. Wada, M. Itoh, N. A. Pertsev, S. van Dijken, and T. Taniyama, "Electric-field switching of perpendicularly magnetized multilayers," NPG Asia Mater. **7**, e198 (2015).
[13]D. Bhattacharya, S. Bandyopadhyay, and J. Atulasimha, "Voltage induced strain control of magnetization: Computing and other applications," Multifunct. Mater. **2**, 032001 (2019).
[14]P. Shepley, A. Rushforth, M. Wang, G. Burnell, and T. Moore, "Modification of perpendicular magnetic anisotropy and domain wall velocity in Pt/Co/Pt by voltage-induced strain," Sci. Rep. **5**, 7921 (2015).
[15]E. D. Ranieri, P. Roy, D. Fang, E. Vehsthedt, A. Irvine, D. Heiss, A. Casiraghi, R. Campion, B. Gallagher, T. Jungwirth *et al.*, "Piezoelectric control of the mobility of a domain wall driven by adiabatic and non-adiabatic torques," Nat. Mater. **12**, 808–814 (2013).
[16]W. Li, B. Buford, A. Jander, and P. Dhagat, "Acoustically assisted magnetic recording: A new paradigm in magnetic data storage," IEEE Trans. Magn. **50**, 37–40 (2014).
[17]L. Thevenard, I. S. Camara, J.-Y. Prieur, P. Rovillain, A. Lemaître, C. Gourdon, and J.-Y. Duquesne, "Strong reduction of the coercivity by a surface acoustic wave in an out-of-plane magnetized epilayer," Phys. Rev. B **93**, 140405 (2016).
[18]W. Edrington, U. Singh, M. A. Dominguez, J. R. Alexander, R. Nepal, and S. Adenwalla, "Saw assisted domain wall motion in Co/Pt multilayers," Appl. Phys. Lett. **112**, 052402 (2018).
[19]A. Adhikari and S. Adenwalla, "Surface acoustic waves increase magnetic domain wall velocity," AIP Adv. **11**, 015234 (2021).
[20]A. Adhikari, E. Gilroy, T. Hayward, and S. Adenwalla, "Surface acoustic wave assisted depinning of magnetic domain walls," J. Phys.: Condens. Matter **33**, 31LT01 (2021).
[21]Y. Cao, X. Bian, Z. Yan, L. Xi, N. Lei, L. Qiao, M. Si, J. Cao, D. Yang, and D. Xue, "Surface acoustic wave-assisted spin–orbit torque switching of the Pt/Co/Ta heterostructure," Appl. Phys. Lett. **119**, 012401 (2021).
[22]J. Dean, M. Bryan, J. Cooper, A. Virbule, J. Cunningham, and T. Hayward, "A sound idea: Manipulating domain walls in magnetic nanowires using surface acoustic waves," Appl. Phys. Lett. **107**, 142405 (2015).
[23]J. Paskauskas, R. Rimeika, and D. Ciplys, "Velocity and attenuation of surface acoustic waves in proton-exchanged 128 degrees-rotated Y-cut $LiNbO_3$," J. Phys. D: Appl. Phys. **28**, 1419 (1995).

[24] T. Nozaki, M. Konoto, T. Nozaki, H. Kubota, A. Fukushima, and S. Yuasa, "Control of the magnetic domain of Pt/Co/Ru/MgO multilayer: Effect of Co thickness and Ru insertion," AIP Adv. **10**, 035130 (2020).
[25] T. Yokouchi, S. Sugimoto, B. Rana, S. Seki, N. Ogawa, S. Kasai, and Y. Otani, "Creation of magnetic skyrmions by surface acoustic waves," Nat. Nanotechnol. **15**, 361–366 (2020).
[26] L. Thevenard, I. S. Camara, S. Majrab, M. Bernard, P. Rovillain, A. Lemaître, C. Gourdon, and J.-Y. Duquesne, "Precessional magnetization switching by a surface acoustic wave," Phys. Rev. B **93**, 134430 (2016).
[27] A. Vansteenkiste, J. Leliaert, M. Dvornik, M. Helsen, F. Garcia-Sanchez, and B. Van Waeyenberge, "The design and verification of Mumax3," AIP Adv. **4**, 107133 (2014).